FINAL REPORT SCEC GRANT 09147

Constraining the Active Fault Configuration in the San Gorgonio Pass Region

Michele Cooke, *University of Massachusetts*

Introduction

The segments of the southern San Andreas Fault (SAF) south of the Cajon Pass have not slipped recently and may be nearing the end of their recurrence intervals (e.g. Yule and Sieh, 2001; McGill et al, 2002; Weldon et al., 2005). Future seismic activity of the southern San Andreas fault system depends not just on activity of the SAF, but also on the interaction among nearby faults such as the San Jacinto fault and faults of the Eastern California Shear Zone (ECSZ) (Fig. 1). In the San Gorgonio Pass region, the SAF is currently composed of several active fault surfaces with complex topology (e.g. *Matti et al*, 1992; *Carena, et al*., 2004; *Langenheim, et al*., 2005; *Langenheim, et al*., 2006; *Yule and Sieh*, 2003; *Dair and Cooke*, 2009; Yule, 2009). Understanding the nature of future earthquakes in this area relies on accurate knowledge of three-dimensional fault configuration and interaction in this region.

Detailed surfaces for active faults in Southern California have been compiled within the SCEC Community Fault Model (*Plesch, et al.*, 2008). Faults of this dataset are defined at the highest resolution available from geologic maps, wells and seismic reflection data. Where subsurface fault configurations are uncertain, the CFM presents alternative models. My students and I have produced numerical models of the San Bernardino region that include the three-dimensional configurations of the active fault surfaces that are available through the CFM (Fig. 2). *Dair and Cooke* (2009) show that three-dimensional representations of the active southern San Andreas, including the north-dipping San Gorgonio thrust are needed to accurately simulate geologic deformation. While, the model of Dair and Cooke (2009) includes only the San Andreas and San Jacinto faults, we now incorporate secondary active faults including the faults of the Eastern California Shear zone, the North Frontal fault, Garlock, Cucamunga and Pinto Mountain faults. We have produced models that simulate both geological time scale (>1000 years) and intersiesmic time scale (<300 years) for comparison of results with geologic slip rates and geodetic data.

Boundary Element Method Modeling

We utilize a three-dimensional Boundary Element Method (BEM) code, Poly3D, that solves the governing differential equations of continuum mechanics (e.g. *Crouch and Starfield*, 1990). BEM codes can simulate the deformation of any homogeneous and isotropic three-dimensional body if either the tractions or displacements are prescribed on the surfaces of that body. Thus, the stress and strain fields throughout the body are uniquely determined by the prescribed boundary conditions (i.e. remote strain and fault tractions). With the Poly3D code, faults within a linear-elastic half-space have either

prescribed slip or are shear stress free. The three-dimensional faults are discretized into two-dimensional triangles each of which has constant slip and opening (*Thomas*, 1993).

Previous Poly3D models of fault systems in southern California using SCEC's CFM have matched well the available geologic slip rates and uplift patterns (*Cooke and Marshall,* 2006; *Griffith and Cooke*, 2004; *Meigs et al*, 2008, *Marshall et al*, 2008; Dair and Cooke, 2009). Because only the faults surfaces are meshed in BEM models, this method avoids the challenge of creating robust volumetric meshes around complex faults encountered when using finite element method (FEM). Furthermore, the triangular elements used in the BEM code preserve the complex topology of fault surfaces documented in the SCEC Community Fault Model. BEM investigations of alternative fault configurations (*Meigs et al, 2008 Griffith and Cooke*, 2004) and varying planarity of faults (*Marshall, et al.*, 2008; *Dair and Cooke*, 2009) demonstrate that the three-dimensional fault geometry and connectivity exhibit first-order effects on the distribution of deformation within these fault systems. Consequently, we expect that geometric irregularities along the active faults of the San Bernardino area will influence local deformation. For this study, we incorporate the preferred fault configurations in the CFM with an average element size of 4.4 km to simulate fault surface irregularities of 10 km or larger. This level of detail is required to investigate the effects of fault geometry and connectivity on deformation.

The numerical models proposed for this study can investigate both geologic time–scale (>1000 years) and interseismic time-scale (< 300 years) deformation. Within the geological time-scale models the faults are free to slip at all depths, whereas with the interseismic time-scale models, the faults are locked within the upper seismogenic crust. Three-dimensional interseismic models of the Los Angeles basin that include geologically reasonable fault configurations show good match to the GPS station velocities with slip rates that also match the geologic rates (*Marshall et al*, 2009). In this study, we apply the approach of *Marshall et al (2009)* to the San Gorgonio Pass region in order to investigate the model match to GPS station velocity.

Present Day Fault Geometry and Slip Rates

The San Andreas Fault

Within southern California, motion along the boundary between the North American and Pacific plates is partitioned among a variety of faults including the San Andreas fault system. The San Andreas fault from the northwest to southeast through the San Gorgonio Knot is comprised of the vertical Mojave segment of the San Andreas, which slips at 24.5 ± 3.5 mm/yr (Weldon and Sieh, 1985) near Cajon Pass where the fault transitions in the sub-vertical San Bernardino strand of the San Andreas fault (Figure 1). The San Bernardino strand of the San Andreas fault is the western boundary of a 20-km-wide restraining bend step over (Figure 1). The San Bernardino strand has been active for the last 125,000 years and has experienced 3 km of horizontal offset (Matti et al., 1985) giving a time averaged slip rate of 24 mm/yr. Estimates of recent slip rate along the San Bernardino strand of the San Andreas fault range between 2.6 and 17

mm/yr (Orozco, 2004; McGill et al., 2006; McGill et al., 2007) with slower slip rates to the south. Though the San Bernardino strand of the San Andreas fault and the San Gorgonio thrust are connected at depth, at the surface the San Bernardino strand turns south-west the near San Gorgonio Canyon and is only indirectly connected with the San Gorgonio thrust via the southern most tip of the Grady Ranch fault (Figure 1; Yule and Sieh, 2003).

The San Gorgonio thrust bounds the restraining bend step-over to the south (Figure 1; Yule and Sieh, 2003). The thrust has a saw-tooth-like geometry (Matti et al., 1985; Matti and Morton, 1993; Yule and Sieh, 2003). The northwest trending segments are oriented parallel to the overall plate motion and accommodate right lateral strike-slip, while the northeast trending segments exhibit reverse slip. The San Gorgonio thrust formed to accommodate contraction and uplift associated with the restraining bend in the San Bernardino Mountain segment of the San Andreas fault (Morton and Matti, 1993). The thrust fault has a strike-slip rate of 5.8 ± 0.8 mm/yr (Yule et al., 2001) and a reverse-slip rate of 1.0-1.3 mm/yr (Matti et al., 1992). The eastern tip of the San Gorgonio thrust connects to the Garnet Hill and Banning strands of the San Andreas fault.

The parallel Garnet Hill fault and the Banning strand of the San Andreas fault are interpreted to merge into one north-dipping fault surface at a depth of 5 km (Figure 1; Yule and Sieh, 2003). Both faults have recent strike-slip rates of less than 1 mm/yr (Langenheim et al., 2005) though the Banning is a older strand of the San Andreas which became reactivated with the new Garnet Hill fault in the present day geometry (Matti and Morton, 1993). Where the Garnet Hill fault/Banning strand of the San Andreas fault connect with the San Gorgonio thrust the structure dips to the north. The Garnet Hill fault/Banning strand of the San Andreas becomes increasingly steep to the southwest and is nearly vertical where the fault merges into the Coachella Valley segment of the San Andreas fault to the south-west.

The Coachella Valley segment of the San Andreas fault is a relatively straight, sub-vertical fault that runs along the eastern shore of the Salton Sea (Figure 3.1; Matti and Morton, 1993). South of the Indio Hills, where the strike-slip rate on the fault is 9 -15 mm/yr (Behr et al., 2007), the fault bifurcates. The south-western fork transitions into the active Garnet Hill/Banning fault zone (Yule and Sieh, 2003). The presently active north-eastern fork, from which the 9-15 mm/yr slip rates is determined, has offset Holocene alluvium (Matti and Morton, 1993; Behr et al., 2007), though at the northern tip of the eastern fork, the fault turns west and becomes inactive (Figure 1; Matti et al., 1985). At this location the eastern fork bifurcates again into two formally active main strands of the San Andreas fault; the Mission Creek strand and the Mill Creek strand.

The San Jacinto Fault

In the San Gorgonio pass region, the San Jacinto fault is a sub vertical fault that runs parallel to the San Andreas fault. The San Jacinto fault formed around 1.5 Mya and is a series of en echelon faults with no concrete evidence of connection with the San Andreas fault at the fault's northern tip (Morton and Matti, 1993).

Eastern California Shear Zone

The Eastern California Shear Zone (ECSZ) is a series of north-south and east-west trending faults located to the north of the San Gorgonio knot that accommodate around 15% of the Pacific/North American right-lateral plate motion (Figure 3.1; Sieh et al., 1993). The combined slip rate of the ECSZ is ≤ 6.2 ± 1.9 mm/yr (Oskin et al., 2008). The faults of the ECSZ were not originally formed in order to accommodate strike-slip motion as they do now, but instead were formed as normal faults during Miocene extension in the Basin and Range province (e.g. Oskin et al., 2008). Recent strike-slip earthquakes that have occurred along the faults of the ECSZ include the Landers earthquake (M_w 7.3) of 1992 and the Hector Mine earthquake (M_w 7.1) of 1999.

The Mojave Desert portion of the ECSZ is separated from the northern portion of the ECSZ by the Garlock fault. The Garlock fault is a left-lateral strike-slip fault that has been active for at least the last 2.2 Ma with a slip rate of 0.7 – 9 mm/yr (Clarke et al., 1984; McGill and Sieh, 1991; McGill and Sieh, 1993) and intersects the San Andreas fault at the Big Bend (e.g. McGill and Sieh, 1991). The Mojave Desert portion of the ECSZ has been actively accommodating right-lateral plate boundary shear for approximately 10 – 6 Ma (Dokka and Tavis, 1990; Oskin and Iriondo, 2004).

The North Frontal Thrust

The south-dipping North Frontal thrust forms the northern boundary of the San Bernardino Mountains. This fault in conjunction with the north-dipping San Gorgonio thrust along the southern front of the range are believe to act in concert to uplift the San Bernardino Mountains. The North Frontal thrust is located to the north of the San Gorgonio thrust and has a dip-slip rate of >0.5 mm/yr for the last 2-3 Ma (Spotila and Sieh, 2000).

Geologic Time-Scale Numerical Models

To simulate geologic time-scale deformation across the southern San Andreas fault system, we apply plate boundary deformations rates to the edges of the model. The displacements are applied along the base of the model and far from the investigated faults. The base of the model is a horizontal crack at 35 km depth that decouples the upper 35 km from the otherwise semi-infinite half-space. We leave the center of the base freely-slipping so that faults near the San Gorgonio Pass can interact without having prescribed rates of slip (Figure 2). The fault surfaces from the SCEC Community Fault Model (Plesch et al., 2007) are only defined to the base of seismicity so we extend these faults through the crust to the horizontal crack. To simulate the regional deformation, we prescribe an overall N52˚W, 45 mm/yr right-lateral displacement onto the outer edges of the detachment to mimic plate motion (e.g. Bennett et al., 1999). The edges of the detachment are far from the San Gorgonio Pass study area in each direction to minimize edge effects (>300 km). If faults extend to the edge of the model, the distal tips are also assigned a strike-slip rate (Figure 2). This prescribed strike-slip at the fault tips is used to simulate infinitely long faults within this finite model. All faults and the detachment are prescribed zero opening in the normal direction to insure the

faults do not open or interpenetrate and are shear-traction free, allowing the faults to slip freely in response to the prescribed displacement and interact with each other. By dictating that the faults be weak in shear throughout the brittle crust, our geologic time-scale model simulates the cumulative interseismic and coseismic deformation within the time modeled. The simulated time for each model is arbitrarily 1000 years. Because the models are elastic, the same geologic slip rate will result from any modeled length of time. The results of three-dimensional BEM models of active faulting above a deep-seated horizontal detachment match well the geologic deformation in southern California (Cooke and Marshall, 2006; Marshall et al., 2008; Meigs et al, 2008; Dair and Cooke, 2009).

Slip rates from the geologic time-scale model

Model strike-slip rates along several faults are compared with geologically observed and interpreted strike-slip rates (Figure 3A). For segments of the San Andreas that have parallel strands, the strike slip along both stands is summed in Figure 3A. Additionally, the strike-slip rate along the eastern branch of the northern fork of the Coachella Valley segment of the San Andreas fault, separate from the western fork, is shown for comparison to the geologic slip rate collected along that strand.

The model predicted right-lateral slip rates along the San Bernardino strand of the San Andreas match well three of the geologic slip rates by Weldon and Sieh (1985) from Lost Lake, Seitz and Weldon (1994) from Pitman Canyon and McGill et al. (2006) from Plunge Creek (Figure 3). The model overestimates right-lateral slip along the San Bernardino segment at Badger Canyon (McGill et al, 2007) and at Burro Flats (Orozco et al., 2004). However, the rate from Burro Flats could be a minimum estimate because there are many active strands in this area. The modeled right-lateral slip rate on the Banning fault matches one of the slip rate estimates of Yule and Sieh (2003) from terraces at Millard Canyon (~5 mm/yr over 100 ka; Figure 3). While the modeled reverse slip rate for the San Gorgonio fault at Millard Canyon is 0.15 mm/yr and much lower than the < 2.5 mm/yr estimated by Yule and Sieh (2003), reverse slip along the modeled fault 5 km to the west of Millard canyon reaches 4.5 mm/yr (Fig 4). Local effects within the model may be suppressing reverse slip at the western end of the San Gorgonio thrust.

The irregular distribution of strike-slip along the San Gorgonio Thrust owes to the scalloped shape of the fault (purple results on Fig. 3). Although the modeled San Gorgonio Thrust has left-lateral slip at the Earth's surface, Yule and Sieh (2003) do not see evidence for left-lateral slip along the San Gorgonio Thrust. This anomalous slip sense is likely an artifact of modeling two proximal, parallel and connected freely-slipping faults. Within 5 km depth in the model the San Gorgonio and Banning faults merge into one active north-dipping structure. The right-lateral slip along the Banning segment of the San Andreas more than compensates for the small amount of left-lateral slip along the San Gorgonio Thrust so that the overall strike slip in the region is right-lateral. Similarly small amounts of normal slip along the Banning strand of the San Andreas fault are more than compensated by reverse slip on the San Gorgonio Thrust.

Generally, our models show partitioning of strain along the Banning strand of the SAF and San Gorgonio Thrust; the San Gorgonio accommodates dip slip and the Banning accommodating predominantly right-lateral slip (Figure 3A and Fig 4). This partitioning follows the geologic evidence for the two faults (Yule and Sieh, 2003).

Along the Eastern Coachella segment of the SAF, the modeled right-lateral slip rates fall within the slip rate range determined by Behr et al (2007) at the Biskra Palms site (Figure 3). The majority of the available geologic strike-slip rate data are well-matched along the modeled San Andreas fault and lead us to conclude that the model captures many of the first-order aspects of deformation within the region.

Where slip along the SAF decreases, slip along the San Jacinto fault increases so that there is a tradeoff in slip rates along these two faults. The modeled right-lateral slip rates along the San Jacinto fault match neither of the available geologic slip rates (Figure 3b). Dair and Cooke (2009) had the same mismatch with models that only included the San Andreas and San Jacinto faults. The mismatch of slip rates along the modeled San Jacinto fault owes to the model's over simplification of the highly echelon geometry of the San Jacinto fault. Further refinement of the model is needed.

We also investigate surface distributions of strike-slip rate at the Earth's surface along a few of the secondary faults in the model (Figure 3). The modeled strike-slip rate distribution along the Garlock fault matches 4 of 7 geologic slip rate sites at the specific study locations, and nearly fits 5 of 7 sites (Figure 3C).

The model reverse-slip along the North Frontal thrust (1.26-3.54 mm/yr) fits the geologic reverse slip rate of >0.5 mm/yr (Figure 4), though this geologic range is broad (Spotila and Sieh, 2000). The modeled dip-slip rates at the Earth's surface along the eastern San Gorgonio thrust (0.08 -6.51 mm/yr reverse slip) overlaps with the geologic dip-slip rate (1.0-1.3 mm/yr; Matti at al., 1992). However, the model also predicts normal sense of slip along the western part of the San Gorgonio thrust fault, inconsistent with geologic and geomorphic observations of recent uplift. Within the model, this region experiences local extension because right lateral slip rates increase along the San Jacinto near the bend of the SAF created by the San Gorgonio fault, where slip rates along the SAF decrease. Normal fault slip is observed in the region along the Crafton Hills fault, but the normal slip along the western San Gorgonio fault is unexpected. We are currently exploring the role of a local mantle drip that has been interpreted from mantle velocities (Faye, 2008) on the deformation of the San Bernardino region. A drip may induce additional compression across the range that may eliminate the normal slip along the western San Gorgonio fault. Additionally, increased segmentation of the San Jacinto fault may also slow slip on this fault so that local extension is reduced.

Interseismic Time-Scale Numerical Models

During the period between earthquakes, faults are not slipping within the seismogenic crust. To simulate interseismic time-scale deformation across the southern San

Andreas Fault system, we apply the geologic slip rates from the geologic time-scale model to the fault surfaces below the locking depth. While above the locking depth, slip on the faults is zero, below the locking depth, the interseismic model has the same slip as the geologic model. In this way, the interseismic model simulates a uniform loading rate at depth equal to the geologic loading rate. The interseismic model approach that we use does not invert for slip; rather, we use the slip from the geologic model and assess the resulting discrepancy of GPS station velocities (Marshall et al, 2009). The advantages of this approach over interseismic models that invert for slip are that 1) we prescribe slip rates that are consistent with the geologic model and 2) that our model incorporates three-dimensional fault surfaces. Incorporating such complex fault configuration is prohibitively difficult with traditional inversion approaches.

The residuals between the model predicted and the GPS station velocities depend on locking depth of the model (Figure 5). Model results were compared to SOPAC rates for stations in the region. Models with 20 km locking depth have the lowest root mean squared while the 20km and 25 km locking depth models have lowest weighted root mean squared. These locking depths match the base of seismicity in the region suggesting that the models are adequately simulating the interseismic deformation.

Model and SOPAC station velocities are plotted with reference to the Yucaipa ridge station (P609), which lies just to the northeast of the active San Bernardino strand of the San Andreas fault (Figure 6A). The model predicted GPS station velocities match very well the SOPAC velocities in most areas of figure 6, except for the zone highlighted in green. Although the model predicts a velocity gradient northeast of the San Andreas from the Yucaipa ridge station (P609), the SOPAC data show very similar velocities for P609 and the BBRY station at Big Bear. This suggests that the crust between these stations is nearly rigid. The uplift of basement rocks within the San Bernardino mountains may increase the effective stiffness of this region. We account for this rigid block by removing the model predicted velocities at BBYR from all stations within the green zone. This green zone includes areas that would have lesser velocity relative to P609 if the zone in yellow were rigid (Figure 6A). The velocity map revised for rigid crust within the San Bernardino mountains has greater match of interseismic model results and SOPAC velocities.

Remaining discrepancies between the orientation of model station vectors with GPS station velocities may be due to a variety of causes including anthropogenic motions within the GPS signal, inaccurate fault representation. Discrepancies in GPS station velocity magnitude may also reflect temporal variations in loading rate on the faults. We are currently investigating the effects of a mantle drip below the San Bernardino mountains (Fay et al, 2008) on intersiesmic deformation.

Conclusion

For most of the region, the modeled geologic slip rates match well the geologic data. Furthermore, modeled slip rate distributions fit spatial variations in slip observed by multiple geologic studies of the same fault. The spatial variance in measured slip rates

along single fault segments, complicates estimation of seismic hazard. How can we known which of the paleoseismic studies produces a slip rate that is representative for the fault segment? An average of the sites can be taken but with low sample, we cannot know that this is representative. In contrast, numerical models simulate the fault with a large number of elements over which a robust average slip rate can be determined. The numerical models that match available geologic rates may provide more robust representative slip rates for the fault than an average of available rates from paleosiesmic studies.

The modeled interseismic velocities match well the GPS station velocities when the crust of the San Bernardino mountains region is considered rigid. Consideration of rigid crust beneath the San Bernardino may be consistent with the evidence that this are is a long-live region of complexity along the San Andreas fault (Matti and Morton, 1993).

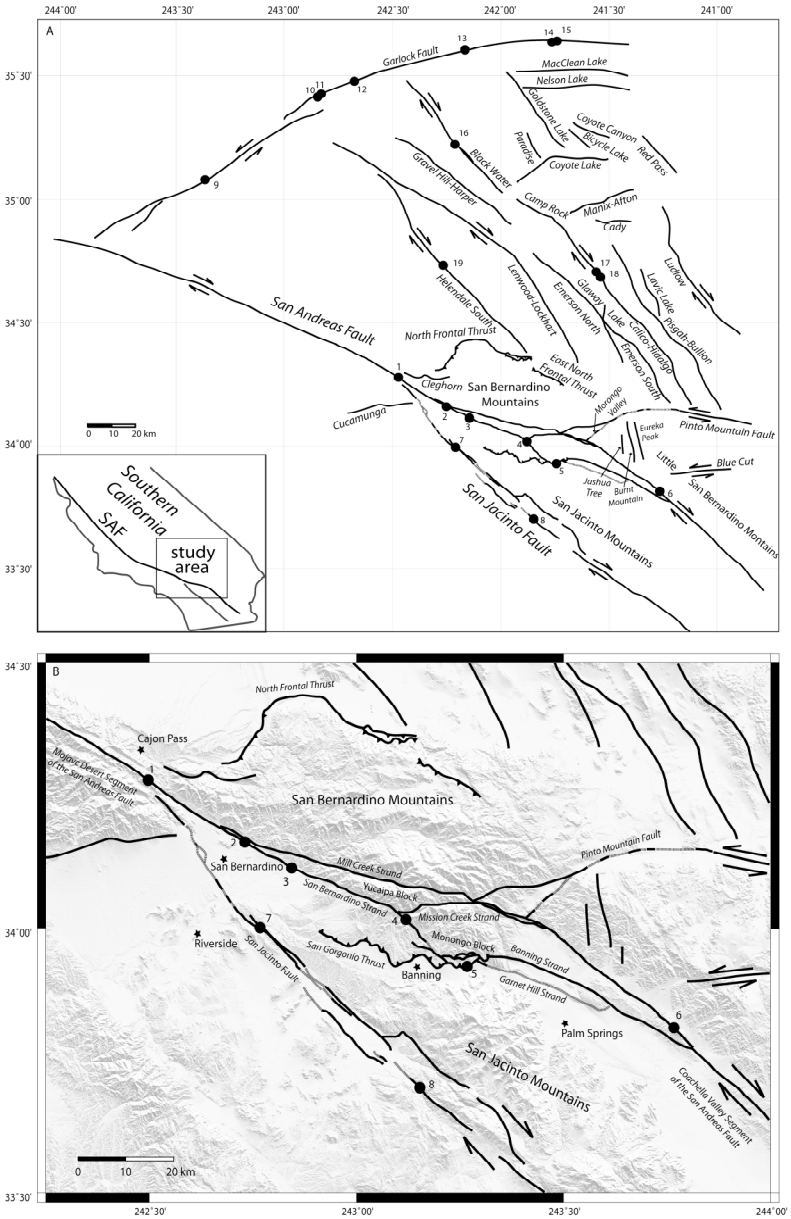

Figure 1. Area maps of the San Bernardino Mountain segment of the San Andreas fault in southern California.The dashed lines indicate faults with no surface trace. Black dots indicate locations of geologic slip rate studies used in model validation. Site 1, Cajon Pass– Weldon and Sieh, 1985; site 2, Badger Canyon– McGill, 2007; site 3, Plunge Creek- McGill et al., 2006; site 4, Burro Flats – Orozco, 2004; site 5, Yule et al., 2001; site 6 - Behr et al., 2007; site 7 - Kendrick et al., 2002; site 8 - Rockwell et al., 1990 and Rockwell, 2006, site 9, 10 and 13– Clarke et al., 1984, site 11, 12 and 14 – McGill and Sieh, 1991, site 15- McGill and Sieh, 1993, site 16- Oskin and Iriondo, 2004, site 17- Oskin et al., 2007, site 18 and 19- Dokka 1983 and Dokka and Travis, 1990. A) contains all of the faults modeled in this study including the Eastern California Shear Zone, which includes all fault from Helendale South eastward. B) shows a close up of the San Bernardino Mountain area and the different fault strands that have been active in the last 500 Ky (modified from Matti et al. 1992).

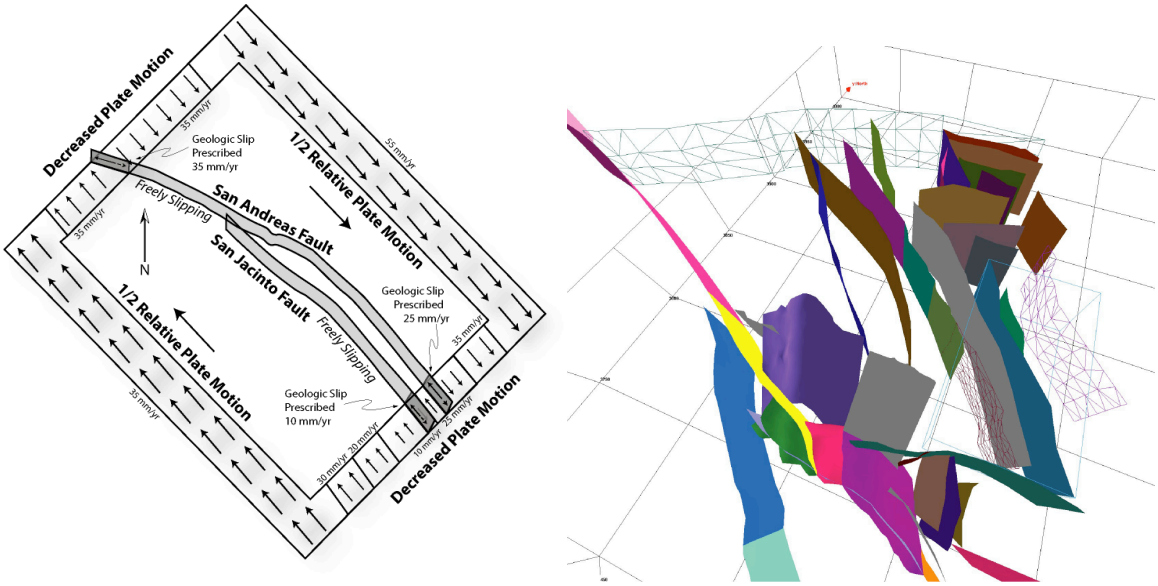

Figure 2. A) A schematic drawing of the loading of the models. The edges of the 35 km deep detachment as well as the distal tips of the primary faults have prescribed slip. The slip on the detachment is decreased incrementally as each section nears the strike-slip fault until slip on the section adjacent to the fault matches the prescribed slip on the fault tip. Slip is prescribed on the eastern edge of the detachment than the western edge due to the plate bounding slip partitioned onto the Eastern California Shear Zone located to the north east of the San Bernardino Mountain segment of the San Andreas fault. In the center of the model, all faults slip and interact in response to the loading at the edges of the detachment. B) Oblique view to the north of all faults in the model. Several faults are shown in wireframe to demonstrate the meshing of the faults.

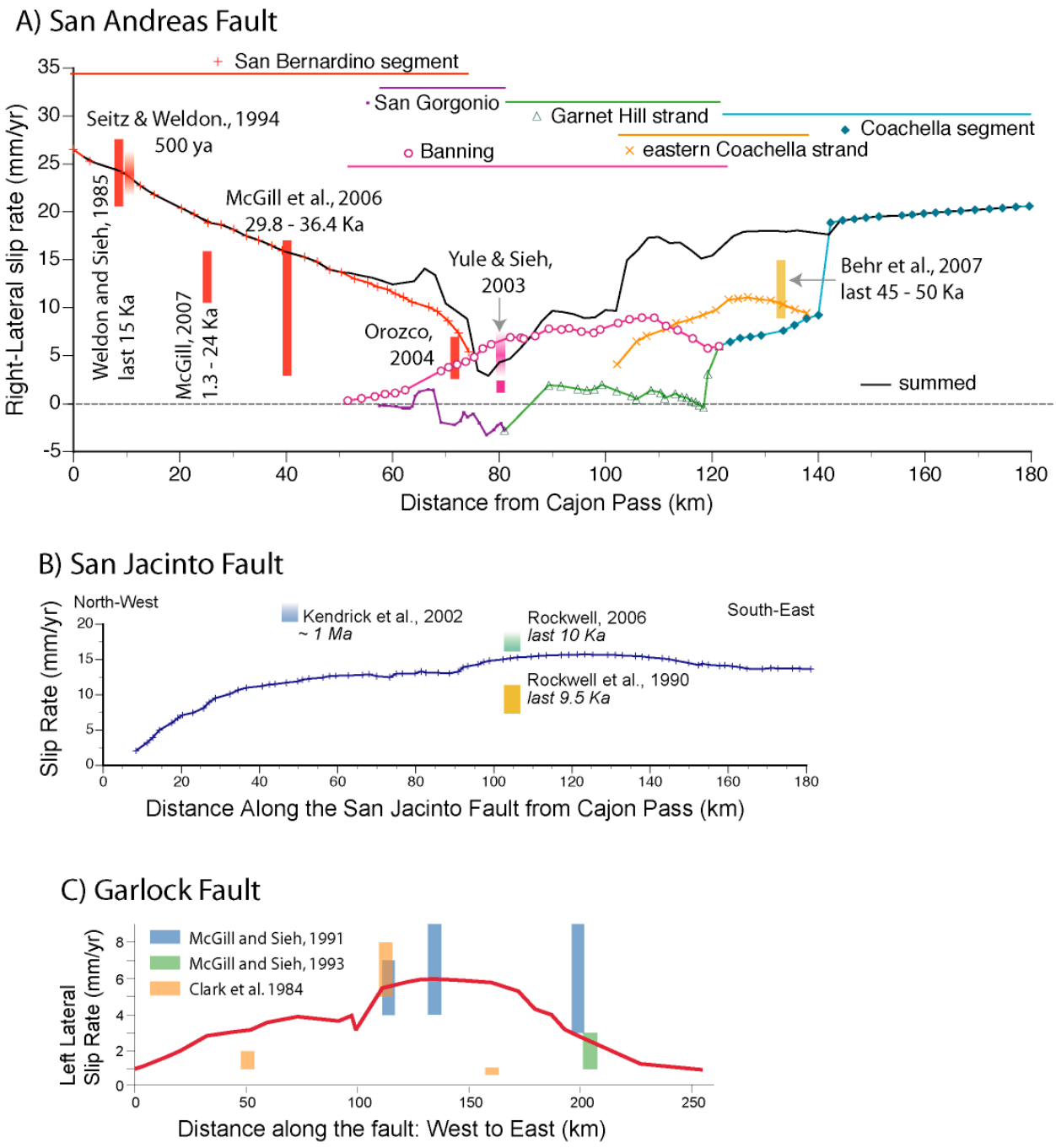

Figure 3: A) Different segments of the San Andreas show in contrasting colors to ease comparison with geologic data for that segment. Strike slip rates along the modeled San Andreas Fault matches well most geologic strike-slip rates. B) The modeled San Jacinto fault strike slip rates do fall within any of the available geologic slip rates. Increased segmentation of the modeled fault may improve match to data. C) The modeled Garlock fault matches many of the geologic strike slip rates and show significant variability in slip rate along strike.

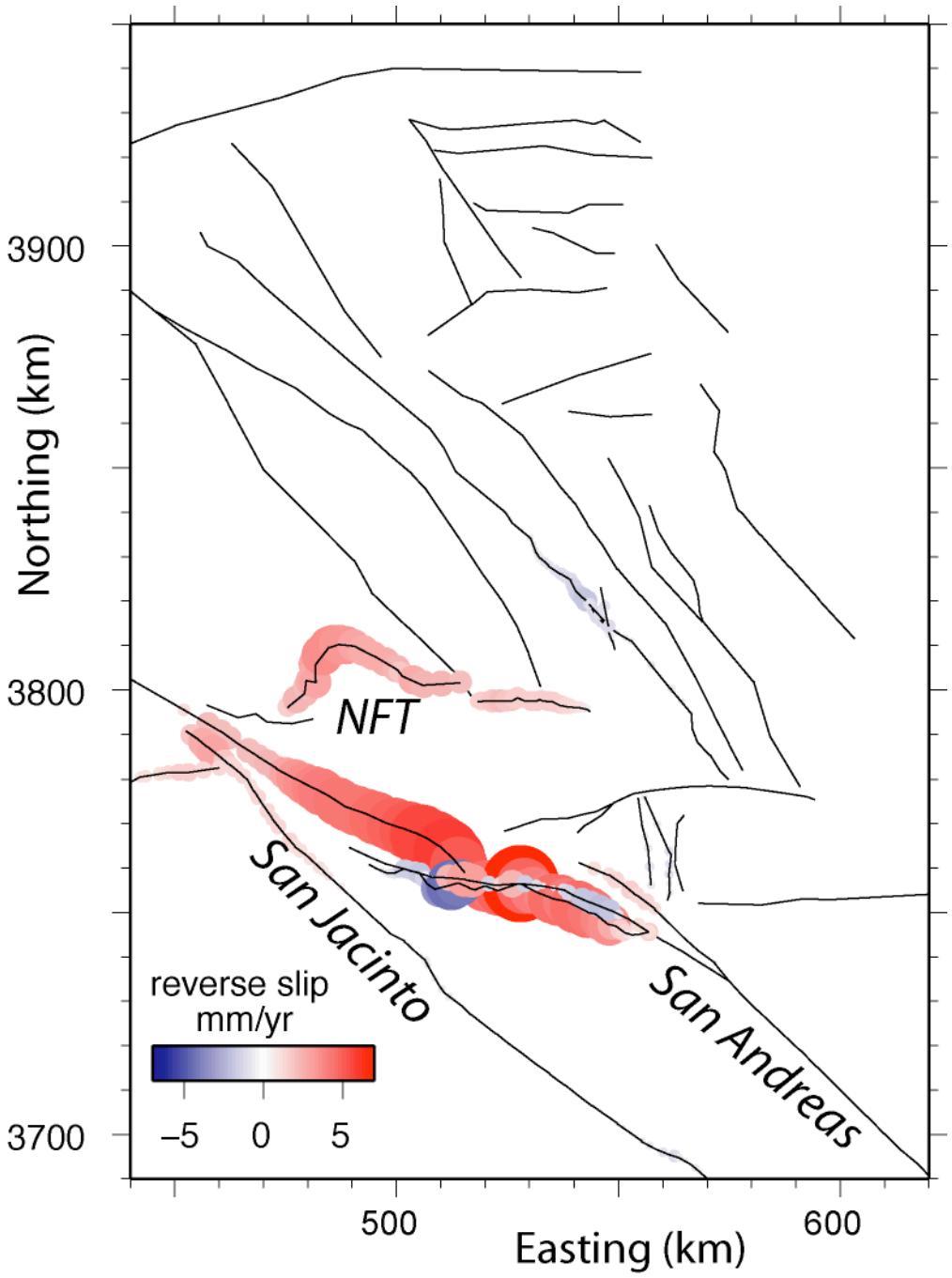

Figure 4: Reverse slip along the north frontal fault, San Gorgonio thrusts and the San Bernardino segment of the San Andreas fault facilitates uplift of the San Bernardino Mountains.

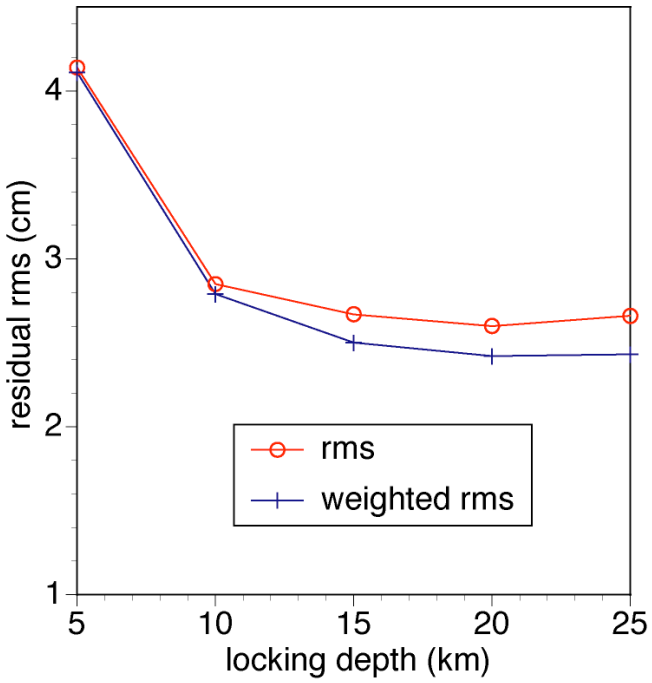

Figure 5: residual RMS and weighted residual RMP for models with various locking depths. The locking depths of 20km have the lowest residuals.

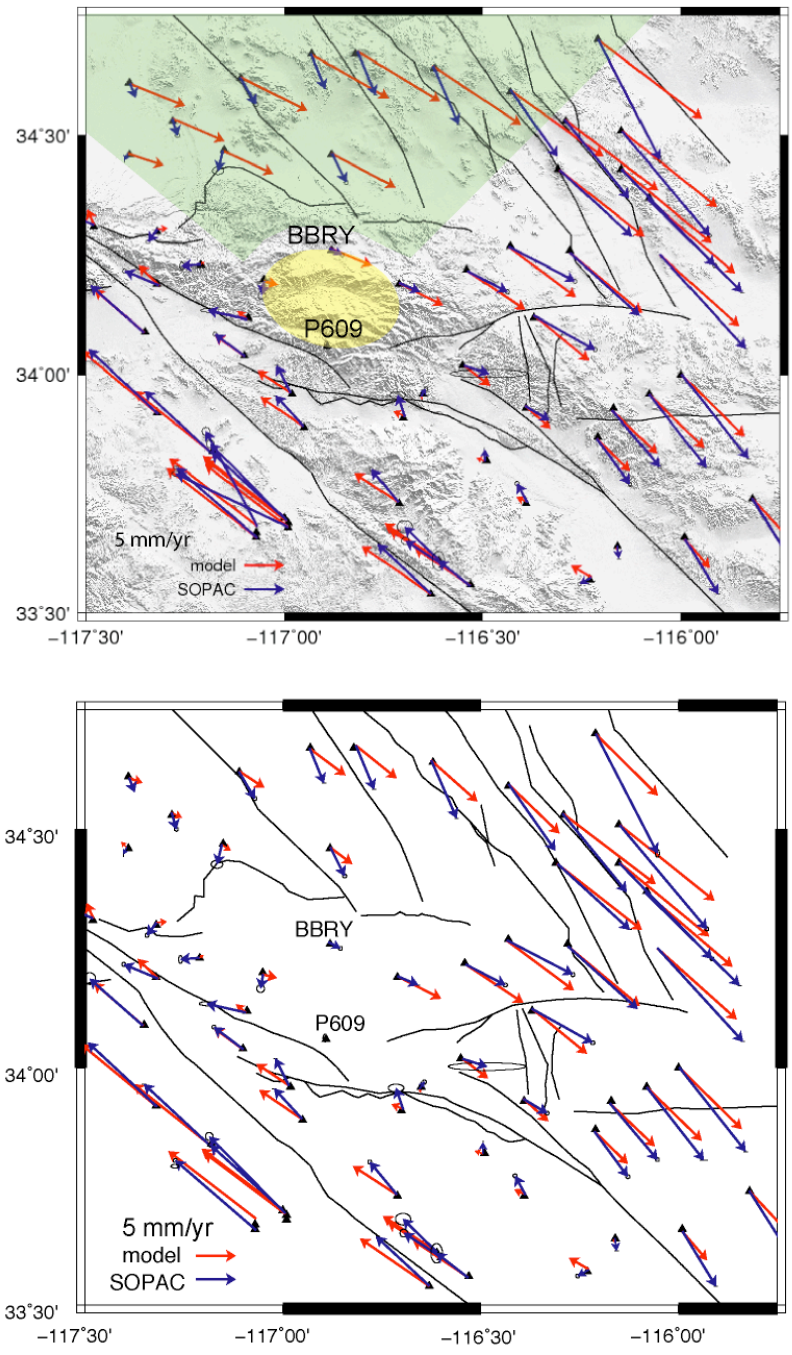

Figure 6: A) Station velocities references to P609 Yucaipa Ridge site with 20 km locking depth. Velocities to the north of the San Bernardino Mts within the green zone have consistent mismatch where as velocities to the south of the San Bernardino Mts have low mismatch. Rigid basement between BBRY and P609 (yellow zone) may resist deformation. B) We remove BBRY velocity from sites in the green zone to simulate rigid material between P609 and BBRY. Removing the BBRY velocity from the sites in the green zone improves the residuals.

References Cited

Allen, C.R., 1957, San Andreas fault zone in the San Gorgonio Pass, southern California: Geological Society of America Bulletin, v. 68, p. 315–350, doi: 10.1130/0016-7606(1957)68[315:SAFZIS]2.0.CO;2.

Anderson, R.S., 1990. Evolution of the northern Santa Cruz Mountains by advection of crust past a San Andreas Fault bend: Science, V. 249, I. 4967, p.397–401.

Behr, W., Hudnut, K., Platt. J., Kendrick, K., Sharp, W., Fletcher K., Finkel, R., and Rood, D., 2007, A revised slip rate estimate for the Mission Creek-Coachella Valley strand of the southern San Andreas fault at Biskra Palms Oasis, Indio, California: Southern California Earthquake Center – Proceedings with Abstracts, v. 17.

Bennett, R.A., Davis, J.L., and Wernicke, B.P., 1999, Present-day pattern of Cordilleran deformation in the western United States: Geology, v. 27, no. 4, p. 371–374, doi: 10.1130/0091-7613(1999)027<0371:PDPOCD>2.3.CO;2.

Bennett, R.A., Friedrich, A.K., and Furlong, K.P., 2004, Codependent histories of the San Andreas and San Jacinto fault zone from inversion of the fault displacement rates: Geology, v. 32, n. 11, p. 961-964, doi: 10.130/G20806.1

Carena, S., Suppe, J., and Kao, H., 2004, Lack of continuity of the San Andreas fault in southern California: Three-dimensional fault models and earthquake scenarios: Journal of Geophysical Research, v. 109, p. B04313, doi: 10.1029/2003JB002643

Clarke, M,M., Harms, K.K., Lienkaemper, J.J., Harwood, D.S., Lajoie, K.R., Matti, J.C., Perkins, J.A., Rymer, M.J., Sarna-Wojcicki, R.V., Sharp, R.V., Sims, J.D., Tinsley, J.C., and Ziony, J.I., 1984, Preliminary slip-rate table for late Quaternary faults of California, US Geologica Survey, Open-File Report, n. 12, p. 84-106.

Crider, J.G., and Pollard, D.D., 1998, Fault linkage: Three-dimensional mechanical interaction between echelon normal faults: Journal of Geophysical Research, v. 103, n. B10, p. 24,373–24,391, doi: 10.1029/98JB01353.

Cooke, M., and Kameda, A., 2002, Mechanical fault interaction within the Los Angeles Basin: A two-dimensional analysis using mechanical efficiency; Journal of Geophysical Research, v. 107, v. B7, doi: 10,1029/2001JB000542.

Cooke, M.L., and Marshall, S.T., 2006, Fault slip rates for three-dimensional models of the Los Angeles metropolitan area, California: Geophysical Research Letters, v. 33, L21313, doi: 10.1029/2006GL027850.

Cooke, M.L., and Murphy, S., 2004, Assessing the work budget and efficiency of fault systems using mechanical models: Journal of Geophysical Research, v. 109, B10408, doi: 10:1029/2004JB002968.

Crouch, S.L., and Starfield, A.M., 1990, *Boundary element methods in solid mechanics: With application in rock mechanics and geologic engineering*: London, Unwin Hyman, 322 p.

Dair, L., and Cooke, M.L., 2009, San Andreas fault geometry through the San Gorgonio Pass, California: Geology. vol. 37; no. 2; p. 119–122; doi: 10.1130/G25101A.1;

Dibblee, T., 1975, Late Quaternary uplift of the San Bernardino Mountains of the San Andreas and related faults: Special Report - California Division of Mines and Geology, v. 118, p. 127–137.

Dokka, R.K., and Travis, C.J., 1990, Late Cenozoic strike-slip faulting in the Mojave Desert, California: Tectonics, v. 9, p. 311-340.

Fay, N.P., Bennett, R.A., and Spinler, J.C., 2008, Small-scale upper mantle convection and crustal dynamics in southern California. G3, v.9, p. 1-23.

Gomez, F., Karam, G., Khawlie, M., McClusky, S., Vernant, P., Reilinger, R., Jaafar, R., Tabet, C., Khair, K., and Barazangi, M., 2007, Global Position System measurements of strain accumulation and slip transfer through the restraining bend along the Dead Sea fault system Lebanon: Geophysical Journal International, v. 168, p. 1021-1028, doi:10.1111/j.1365-246X.2006.03328.x.

Griffith, W. A., and Cooke, M.L., 2004, Mechanical validation of the three-dimensional intersection geometry between the Puente Hills blind-thrust system and the Whittier fault, Los Angeles, California: Bulletin of the Seismological Society of America, v. 94, p. 493-505.

_____ 2005, How sensitive are fault slip rates in the Los Angeles to tectonic boundary conditions?: Bulletin of Seismological Society of America, v. 95, p. 1263 – 1275.

Harris, R.A., Archuleta, R.J., and Day, S.M., 1991, Fault steps and dynamic rupture process: 2-d numerical simulations of a spontaneously propagating shear fracture: Geophysical Research Letters, v. 18, p. 893–896, doi: 10.1029/91GL01061.

Kendrick, K.J., Morton, D.M., Wells, S.G., and Simpson, R.W., 2002, Spatial and temporal deformation along the northern San Jacinto fault, southern California; implications for slip rates: Bulletin of the Seismological Society of America, v. 92, i. 7, p. 2782–2802.

Langenheim, V.E., Jachens, R.C., Matti, J.C., Hauksson, E., Morton, D.M., and Christensen, A., 2005, Geophysical evidence for wedging in the San Gorgonio Pass structural knot, souther San Andreas fault zone, southern California: Geological Society of America Bulletin, v. 117, n. 11/12, p. 1554-1572, doi: 10.1130/B25760.1.

Magistrale H., Day, S., Clayton, R.W., and Graves, R., 2000, The SCEC southern California reference three-dimensional seismic velocity model version 2: Bulletin of the Seismological Society of America 90, p. S65 – S76.

Marshall, S.T., Cooke, M.L., and Owen, S.E., 2008, Effects of nonplanar fault topology on mechanical interaction on fault-slip distributions in the Ventura Basin, California: Bulletin of Seismological Society of America, v. 98, n. 3, p. 1113-1127, doi: 10.1785/0120070159.

Marshall, S. T., M. L. Cooke, and S. E. Owen, 2009. Interseismic deformation associated with three-dimensional faults in the greater Los Angeles region, California, J. Geophys. Res., 114, B12403, doi:10.1029/2009JB006439.

Matti, J.C., and Morton, D.M., 1993, Paleographic evolution of the San Andreas fault in Southern California: A reconstruction based on new cross-fault correlation: in Powel, R.E., Weldon, R.J.II, and Matti, J.C., eds., The San Andreas Fault System: Displacement, Palinspastic Reconstruction, and Geologic Evolution: Boulder Colorado, Geological Society of America Memoir 178.

Matti, J.C., Morton, D.M., and Cox, B.F., 1985, Distribution and geologic relations of fault systems in the vicinity of the central Transverse Ranges, southern California: US Geological Survey Open-File Report 85–365, 23 p.

_____ 1992, The San Andreas fault system in the vicinity of the central Transverse Ranges province, southern California: US Geological Survey Open-File Report 92–354, 52 p.

McGill, S., Kendrick, K., and Weldon, R.J., II, and Owen, L., 2007, Pleistocene and Holocene slip rate of the San Andreas fault at Badger Canyon, San Bernardino, California: Southern California Earthquake Center – Proceedings with Abstracts, v. 17.

McGill, S.F., and Sieh, K.E., 1991, Surficial offsets on the central and eastern Garlock fault associated with prehistoric earthquakes: Journal of Geophysical Research, v. 96, p. 21,597-21,621.

_____ 1993, Holocene slip rates of the central Garlock fault in southern Searles Valley, California: Journal of Geophysical Research, v. 98, n. B8, p. 14,217-14,231.

McGill, S., Weldon, R.J.I.I., Kendrick, K., and Owen, L., 2006, Late Pleistocene slip rate of the San Bernardino strand of the San Andreas fault in Highland: possible

confirmation of the low rate suggested by geodetic data: Seismological Research Letters, v. 77, no. 2, p. 279.

Meade, B.J., and Hager, B.H., 2005, Block models of crustal motion in southern California constrained by GPS measurements: Journal of Geophysical Research, v. 110, p. B03403, doi: 10.1029/2004JB003209.

Meigs, A.J., Cooke, M.L., and Marshall, S.T., 2008, Using vertical rock uplift patterns to constrain the three-dimensional fault configurations in the Los Angeles Basin: Bulletin of Seismological Society of America, v. 98, n. 2, p. 106-123,doi: 10.1785/0120060254.

Meisling, K.E., 1984, Neotectonics of the north frontal fault system of the San Bernardino Mountains, southern California, Ph.D. Thesis, California Institute of Technology, Pasadena, 394 p.

Morton, D.M., and Matti, J.C., 1993, Extension and contraction within an evolving divergent strike-slip fault complex: the San Andreas and San Jacinto fault zone at their convergence in southern California: *in* Powel, R.E., Weldon, R.J.II, and Matti, J.C., eds., The San Andreas Fault System: Displacement, Palinspastic Reconstruction, and Geologic Evolution: Boulder Colorado, Geological Society of America Memoir 178.

Muller, J.R., and Aydin, A., 2003, Using geomechanical modeling to constrain the 3-D fault geometry within the Marmara Sea, Turkey: Geological Society of America, Abstracts with Programs, v. 35, i. 6, p. 40.

Nicholson, C., 1996, Seismic Behavior of the Southern San Andreas Fault zone in the Northern Coachella Valley, California: comparison of the 1948 and 1986 earthquake sequences: Bulletin of the Seismological Society of America, v. 86, n. 5, p. 1331-1349.

Olsen, K.B., Day, S.M., Minster, J.B., Cui, Y., Chourasia, A., Okaya, D., Meachling, P., Jordon, T., 2008, Terashake2; Spontaneous *rupture simulations* of Mw 7.7 earthquakes on the southern San Andreas Fault: Bulletin of the Seismological Society of America, v. 98, i. 3, p. 1162-1185.

Orozco, A.A., 2004, Offset of a mid-Holocene alluvial fan near Banning, CA; constraints on the slip rate of the San Bernardino strand of the San Andreas fault, Master's Thesis, 56 p., University of California at Northridge, Northridge, California.

Oskin, M., and Iriondo, A., 2004, Large-magnitude transient strain accumulation on the Blackwater fault, eastern California shear zone: Geology, v. 32, p. 313-316.

Oskin, M., Perg, L., Shelef, E., Strane, M., Gurney, E., Singer, B., and Zhang, X., 2008, Elevated shear zone loading rate during an earthquake cluster in eastern California: Geology, v. 36, n. 6, p. 507-510.

Plesch, A., and 27 others, 2007, Community fault model (CFM) for southern California: Bulletin of the Seismological Society of America, v. 97, no. 6, p. 1793–1802, doi: 10.1785/0120050211.

Pollard, D.D., Maerten, F., Maerten, L., Resor, P.G., Fiore, P.E., 2002, Forward 3D modeling of complex fault systems using an elastic boundary element method: Geological Society of America, Abstracts with Programs, v. 34, i. 6, p. 251.

Rockwell, T., Loughman, C., and Merifield, P., 1990, Late quaternary rate of slip along the San Jacinto fault zone near Anza, southern California: Journal of Geophysical Research, v. 95, B6, p. 8593–8605, doi: 10.1029/JB095iB06p08593.

Shen, Z.K., Agnew, D.C., King, R.W., Dong, D., Herring, T.A., Wang, M., Johnson, H., Anderson, G., Nikolaidis, R., van Domselaar, M., Hudnut, K.W., and Jackson, D.D., 2003, The SCEC crustal motion map, version 3.0: Los Angeles, California, Southern California Earthquake Center.

Sieh, K., Jones, L., Hauksson, E., Hudnut, K., Eberhart-Phillips, D., Heaton, T., Hough, S., Hutton, K., Kanamoi, H., Lilje, A., Lindvall, S., McGill, S., Mori, J., Rubin, C., Spotila, J., Stock, J., Kie Thio, H., Treiman, J., Wernicke, B., Zachariasen, J., 1993, Near-field investigations of the Landers earthquake sequence, April to July 1992: Science, v. 260, p. 171-175.

Smith, B.R., and Sandwell, D.T., 2003, Coulomb stress accumulation along the San Andreas Fault system: Journal of Geophysical Research, v. 108, n. B6, 2296, doi:10.1029/2002JB002136.

_____ 2006, A model of the earthquake cycle along the San Andreas Fault System for the last 1000 years: Journal of Geophysical Research, v. 111, p. B01405, doi: 10.1029/2005JB003703.

Spotila, J.A., Farley, K.A., and Sieh, K., 1998, Uplift and erosion of the San Bernardino Mountains associated with transpression along the San Andreas fault, California, as constrained by radio helium thermochronometry: Tectonics, v. 17, n. 3, p. 360-378.

Spotila, J.A., Farley, K.A., Yule, J.D., and Reiners, P.W., 2001, Near-field transpressive deformation along the San Andreas fault zone in southern California, based on exhumation constrained by (U-Th)/He dating: Journal of Geophysical Research, v. 106, n. B12, p. 30909–30922, doi: 10.1029/2001JB000348.

Spotila, J.A., Niemi, N., Brady, R., House, M., and Buscher, J., 2007, Long-term continental deformation associated with transpressive plate motion: The San Andreas fault: Geology, v. 35, no. 11, p. 967–970, doi: 10.1130/G23816A.1.

Spotila, J.A., and Sieh, K., 2000, Architecture of transpressional thrust faulting in the San Bernardino Mountains, southern California, from deformation of a deeply weathered surface: Tectonics, v. 19, no. 4, p. 589–615, doi: 10.1029/1999TC001150.

Thomas, A.L., 1993, POLY3D: A three-dimensional, polygonal element, displacement discontinuity boundary element computer program with applications for fractures, faults, and cavities in the Earth's crust, Master's thesis, 52 p., Stanford University., Stanford, California.

Wald, D.J., and Heaton, T.H., 1994, Spatial and temporal distribution of slip for the Landers, California, earthquake: Bulletin of the Seismological Society of America, v. 84, p. 668–691.

Weldon, R., Fumal, T., Biasi, G., 2004, Wrightwood and the earthquake cycle: what a long recurrence record tells up about how faults work: GSA Today, v. 14, n. 9, doi: 10.1130/1052-5173(2004)014.

Weldon, R., Fumal, T., Biasi, G., and Sharer, K., 2005, Past and Future Earthquakes on the San Andreas Fault: Science, v. 308, p. 966–967, doi: 10.1126/science.1111707.

Weldon, R.J., II, and Sieh, K., 1985, Holocene rate of slip and tentative recurrence interval for large earthquakes on the San Andreas fault, Cajon Pass, southern California: Geological Society of America – Bulletin, v. 96, p. 793–812.

Yule, J., Fumal, T., McGill, S., and Seitz, G., 2001, Active tectonics and paleoseismic record of the San Andreas fault, Wrightwood to Indio: working toward a forecast of the next "Big Event": Geologic Excursions in the Californian Deserts and Adjacent Transverse Ranges, edited by Dunne, G., and Cooper, J., Pacific Section, Society of Economic Paleontologists and Mineralogists, Los Angeles, California, p. 91–126.

Yule, D., Sieh K., 2003, Complexities of the San Andreas fault near San Gorgonio pass: Implications for large earthquakes: Journal of Geophysical Research., v. 109, n. B11, 2548, doi: 10.1029/2001JB000451.

Yule, D, 2009. The enigmatic San Gorgonio Pass, *Geology*, vol.. 37; no. 2; p. 191–192; doi: 10.1130/focus022009.1.